IEEE INSTRUMENTATION & MEASUREMENT SOCIETY

Received 28 June 2023; accepted 23 July 2023. Date of publication 8 August 2023; date of current version 29 August 2023.
The review of this paper was arranged by Associate Editor Amitava Chatterjee.

*Digital Object Identifier 10.1109/OJIM.2023.3302908*

# Bilateral Symmetry-Based Abnormality Detection in Breast Thermograms Using Textural Features of Hot Regions

**ANKITA DEY (Graduate Student Member, IEEE), EBRAHIM ALI (Graduate Student Member, IEEE), AND SREERAMAN RAJAN (Senior Member, IEEE)**

Department of Systems and Computer Engineering, Carleton University, Ottawa, ON K1S 5B6, Canada

CORRESPONDING AUTHOR: A. DEY (e-mail: ankitadey@cmail.carleton.ca)

This work was supported by the Natural Sciences and Engineering Research Council of Canada (NSERC).

**ABSTRACT** With an increase in the number of breast cancer cases worldwide, there is an urgent need to develop techniques for early abnormality detection. Thermography is known for its potential to detect breast abnormalities at an early stage. A novel threshold-based non-machine learning asymmetry analysis using textural features is proposed for breast abnormality detection. Breast abnormalities are indicated by regions of elevated temperatures (hot regions), usually, indicated by red color in thermograms. In this work, the breast thermograms are segmented to extract breast tissue profiles and then the red-plane of an RGB thermogram is utilized to analyze the natural contralateral symmetry between the left and right breast of an individual. A novel textural feature based on histogram similarity along with known textural features, such as fractal dimension, hurst exponent, spectral norm, and Frobenius norm, are used as features for asymmetry analysis. Bilateral ratios (BRs) of these features indicate contralateral symmetry between the left and right breast. A BR value closer to 1 indicates such symmetry. Hard voting is done among all the BRs of the textural features to estimate asymmetry between the left and right breast and detect an individual with breast abnormality. The proposed methodology is evaluated on publicly available datasets. It outperforms the state-of-the-art and achieves an accuracy of 96.08%, sensitivity of 100%, and specificity of 93.57%. A comparative analysis of statistical and textural features has also been demonstrated. A novel singular value decomposition (SVD)-based abnormal breast detection technique has been proposed with evaluations on a limited dataset.

**INDEX TERMS** Bilateral symmetry, breast cancer, red-plane, statistical analysis, textural analysis, thermograms.

## I. INTRODUCTION

ACCORDING to the World Health Organization (WHO), globally, breast cancer forms 12% of all annual cancer cases, making it the most frequently diagnosed cancer worldwide [1]. Breast cancer has a mortality rate of 19.47%, however, when detected early has a 5-year survival rate of 99% [2]. Mammography, a radiation-based breast imaging modality, is the gold standard for breast cancer detection. However, mammography has shown reduction in sensitivity of tumor detection from 98% in fatty breast to less than 48% in dense breast in younger women [3]. Ionizing radiation involved in mammography makes it unsuitable for the detection of breast abnormalities during pregnancy.

Thermography, a contact-less, painless, and nonionizing breast imaging modality, can detect abnormalities at precancerous and cancerous stage in both fatty and dense breast. It is an FDA (U.S. Food and Drug Administration) approved adjunctive screening tool that may be particularly useful in resource-lacking remote area hospitals or clinics. A tumor in breast increases the rate of formation of new blood vessels from the preexisting ones (known as Angiogenesis) to meet the need of continuous supply of oxygen and nutrition required for its growth. This process of new blood

**TABLE 1.** Recent state-of-the-art asymmetry-based breast abnormality detection.

| Ref | Type of features used | Classifier | Image domain | Dataset | Performance |
|---|---|---|---|---|---|
| [7] | Curvelet transform based GLCM textural and statistical features of ROI within breast thermograms | SVM | Gray | Private: 22 | Acc: 90.91%<br>Sen: 81.82%<br>Spec: 100% |
| [8] | GLCM textural and statistical features of ROI within breast thermograms | SVM | Gray | Private: 36 | Acc: 83.30%<br>Sen: 83.30%<br>Spec: 83.30% |
| [9] | GLCM textural and statistical features of breast thermograms | Hybrid classifier ensemble | NA | Private:146 | Acc:88.17%<br>Sen: 83.30%<br>Spec: 89.44% |
| [10] | GLCM textural and statistical features of ROI within breast thermograms | SVM | Gray | DMR: 63 | Acc: 88.41% |
| [11] | GLCM textural and statistical features of breasts segmented using bifurcation line | SVM | Gray | DMR: 80 | Acc: 90%<br>Sen: 87.50%<br>Spec: 92.50% |
| [12] | Difference of GLCM matrices and Markov random field (MRF)-based textural features | Hidden Markov model | Gray | Private: 65 | Acc: 93.75%<br>Sen: 95%<br>Spec: 92% |
| [13] | Statistical features of ROI within breast thermograms extracted using block variance | ANN | LAB colour space | DMR: 100 | Acc: 90%<br>Sen: 95%<br>Spec: 85% |
| [14] | Wavelet transform based and curvelet transform based textural features of ROI within breast thermograms | Multiple classifiers | Gray | Private: 81 | Acc: 88%<br>Sen: 81%<br>Spec: 82% |
| [15] | Statistical features of breasts segmented using infra-mammary line | SVM | Gray | DMR: 60 | Acc: 95%<br>Sen: 97.05%<br>Spec: 92.3% |
| [16] | Local instant and center-symmetric neighbor-based histogram features | Broad learning | Gray | Private: 120 | Acc: 94%<br>Sen: 92.7%<br>Spec: 95.5% |

vessels formation increases the skin surface temperature [4]. Thermography is a functional imaging modality that helps in the identification of abnormal regions based on the magnitude of skin temperature gradients [5]. The regions of elevated temperature (or abnormal regions) appear as bright spots or hot spots in breast thermal images. Thermography can detect an abnormal increase in temperature of the breast tissue about 8–10 years before mammography can even detect a mass [6].

A healthy individual has contralateral symmetrical breasts, that is, the temperature distribution of both breasts is almost the same. Synchronous bilateral breast cancer (SBBC) or both breast cancerous is a clinical rarity and occurs only in 2.3% of the diagnosed cases [17]. Thus, asymmetrical temperature distribution between the breasts of an individual may indicate the presence of an abnormality. The majority of the work present in the literature exploits this concept of asymmetry by calculating the difference of statistical and textural features between both the breasts in a given breast thermogram for breast abnormality detection. The state-of-the-art asymmetry based-breast abnormality detection methods utilize these discriminative handcrafted statistical and textural features for traditional machine-learning models, such as support vector machine (SVM), *K*-means, and artificial neural network (ANN) [18]. Deep learning techniques, such as convolutional neural networks (CNNs), have also been implemented for abnormality detection. A summary of the most recent asymmetry-based state-of-the-art papers is given in Table 1. These machine-learning and deep-learning-based methods are data hungry and require a large amount of data to produce reliable results. However, due to the lack of large benchmark datasets, it is observed in Table 1, the sample size of training and testing data used in the existing works is small, leading to overclaimed and unreliable accuracy results [19]. Therefore, there is a pressing need either to develop a large benchmark breast thermogram dataset for proper training and testing or to develop better non-machine-learning techniques. In this work, a threshold-based non-machine learning method that uses textural features for asymmetry analysis is proposed. This work is a novel pilot study conducted to evaluate the feasibility of the proposed non-learning-based technique for breast abnormality detection using thermograms. To the best of the author's knowledge, no work existing in the literature has explored non-learning-based breast abnormality detection techniques.

The discriminative handcrafted features that have been used for breast abnormality detection can either be statistical or textural. Gogoi et al. [20] used the mean difference of discriminative statistical (7 features) and gray-level covariance matrix (GLCM) textural features (17 features) of the left and right breast to detect abnormal breast thermograms using traditional machine-learning (ML) models. The nonuniformity in thermograms causes a large variation in statistical and textural values from one thermogram to the other, therefore, the mean differences of these features may not be the best measure for asymmetry analysis. Realizing this, in this work, bilateral ratios (BRs) of textural and statistical features for asymmetry analysis have been used. The BRs

will always be close to 1 if the breasts are symmetrical irrespective of feature values thus considering the nonuniformity of the thermograms.

Abnormalities in a breast, both benign and malignant, have a definite geometry or patterns. Thus, fractal-based textural features can be used to identify these patterns as opposed to conventional GLCM textural features. Hakim and Awale [21] used fractal textural features, such as fractal dimension (FD), Hurst exponent (HE), and lacunarity for asymmetry analysis and achieved better classification results than with the conventional textural and statistical features. However, these classification results in [21] may be unreliable as they were obtained using traditional machine-learning algorithms with textural features obtained from a small dataset with limited number of samples. Following [21], this work has also utilized fractal-based textural features, such as FD and HE along with other matrix similarity identifying textural features, such as spectral norm and Frobenius norm. A new textural feature for asymmetry analysis called histogram similarity has also been introduced. The correlation between the histograms of symmetrical left and right breast of a healthy individual is high. This correlation is, therefore, used as a measure of asymmetry in this work.

As observed from Table 1, the majority of the state-of-the-art works use grayscale breast thermograms for abnormality detection. A comprehensive review of the existing works in [19] also shows that out of 38 works presented therein, 28 of them process grayscale images while the rest uses RGB thermograms. Thermograms are diffused RGB images where temperature distributions are shown using user-chosen thermal color palettes. Thus, color pixel intensities in thermograms contain abnormality information and converting them into grayscale cause a considerable loss of information. Based on the thermal palettes, the color plane containing abnormality information differs. The Database for Mastology Research (DMR) dataset and Ann Arbor thermography dataset follows the rainbow thermal palette of FLIR [22] where warm colors represent the hottest part of the image while cool colors represent the coldest parts. Both datasets have abnormality information in the red color plane. Thus, in this work, the red-plane of the thermograms is extracted for asymmetry analysis using textural features. Notably, no work existing in the literature utilizes red-plane (hot regions) thermograms for breast abnormality identification.

This article is an extension of our previous work [23] where red-plane asymmetry analysis using statistical features was introduced. In this work, a novel threshold-based non-machine learning methodology for breast abnormality detection that uses textural features for asymmetry analysis of hot regions is proposed. This methodology begins with the extraction of the hot regions (red-plane) of breast thermograms, followed by preprocessing (breast segmentation, noise removal, and contrast enhancement) of the extracted the red-plane of the breast thermogram. The preprocessed thermogram is then divided into left and right breast and the statistical and textural features are extracted from either side. BRs of all features are calculated for either side of the breast and a hard voting is done among them to determine contralateral symmetry. A complete analysis of the effects of the threshold values (determining the contralateral symmetry) on the performance of the proposed methodology is presented. The proposed methodology performs light computations with better accuracy and significantly greater speed than standard ML and deep-learning methods.

The following are the contributions of this article.

1) Introduction of hot-region extraction (red-plane extraction) for asymmetry analysis of breast thermograms using textural features.
2) Proposal of a novel threshold-based non-machine learning method for breast abnormality detection using textural features.
3) Introduction of histogram similarity as a potential textural feature for asymmetry analysis.
4) Detailed comparative analysis of statistical and textural features for grayscale and red-plane images.
5) Proposal of novel singular value decomposition (SVD)-based method for identification of the abnormal breast of a subject, once the subject is considered as having an abnormal breast.

This article is arranged in the following manner. Section II provides the details of the proposed methodology. Section III describes the dataset, the experimental approach, and the results. Section IV introduces the method of identification of abnormal breast for a subject identified as having an abnormality in one of their breasts. Section V presents a detailed comparison of the proposed methodology with the current state-of-the-art. Section VI concludes this article.

## II. PROPOSED METHODOLOGY

A flowchart of the various steps of the proposed threshold-based non-machine learning methodology to analyze the classification performance using statistical and textural features is shown in Fig. 1. Subsequent sections describe each step in detail.

### A. PREPROCESSING

#### 1) HOT-REGION EXTRACTION

An increase in metabolic activity is observed in a developing breast tumor that elevates the temperature of the surrounding tissue and the skin surface. This localized elevated temperature of the breast tissue is detected with the help of infrared cameras during thermal imaging and appears as bright spots or hot spots in a breast thermogram. A healthy subject exhibits thermal symmetry between a particular region of body under study and its contralateral regions. According to the American Academy of Thermology (AAT), the temperature difference between the contralateral breast should not exceed 1.5 °C while the temperature difference between the contralateral nipple should not exceed 1 °C [24]. Typically, breast thermograms are pseudo-colored images employing a

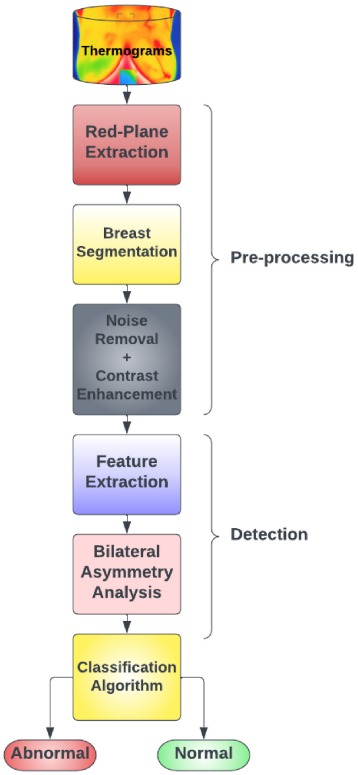


**FIGURE 1.** Proposed methodology.

color gradient palette that displays a temperature range of 8–10 degrees and is capable of detecting up to 0.05 °C thermal difference. The regions of higher temperature or hotspots can be identified based on color gradients in the pseudo-colored breast thermogram. The thermograms in the datasets used in this work have employed a rainbow color palette [22] which represents hot regions by bright colors (such as red) and cold regions by dark colors (such as blue). These thermograms have a range of 8 degrees (27 °C to 35 °C) and a color map of 16 colors. The red regions or hotspots have an elevated temperature between 34 °C and 35 °C which may indicate the presence of an abnormality. Therefore, to facilitate the identification of subjects with abnormal breasts, in this work, the red-plane of the RGB breast thermogram is extracted for further processing. This extracted red-plane highlights the thermal asymmetry in subjects with abnormal breasts as shown in Fig. 2. An input thermogram RGB (three channels) $I_{\text{rgb}} \in \mathbb{R}^{(P\times Q\times 3)}$ can be split into three single-channel images, that is, red-plane image $I_{\text{red}} \in \mathbb{R}^{(P\times Q)_1}$, green plane image $I_{\text{green}} \in \mathbb{R}^{(P\times Q)_2}$, and blue plane image $I_{\text{blue}} \in \mathbb{R}^{(P\times Q)_3}$. Here, $P$ and $Q$ denote the width and height of the input RGB thermogram, respectively.

### 2) BREAST SEGMENTATION

A two-step breast segmentation algorithm [25] that extracts the breast tissue profile from the background as well as from the pectoral muscles is adopted in this work. This

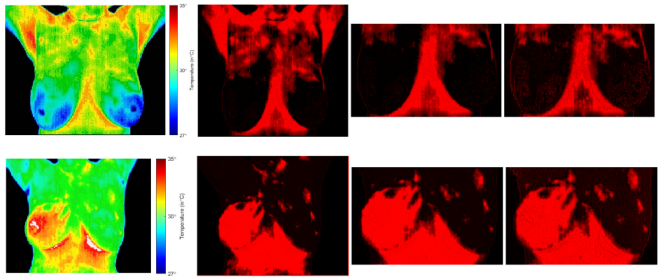

**FIGURE 2.** Breast thermograms of (upper row) (a) normal subject, (b) extracted red-plane of the subject with normal breast, (c) segmented breast tissue profile, (d) filtered breast tissue profile (lower row), (e) abnormal subject, (f) extracted red-plane of the subject with abnormal breast, (g) segmented breast tissue profile, and (h) filtered breast tissue profile.

algorithm is based on Otsu's thresholding [26] and seeded region growing [27] technique.

Otsu's thresholding is an iterative variance-based technique for choosing an optimal threshold $t$ (which is within the range of 0–255) to distinguish the foreground from the background by minimizing the weighted intraclass variance between the foreground and the background. This intraclass variance is given as

$$\sigma^2 = w_{bg}\sigma_{bg}^2 + w_{fg}\sigma_{fg}^2 \tag{1}$$

where $w_{bg}$ and $\sigma_{bg}^2$ represent the pixel probabilities and variance of background pixel class, respectively (both above the threshold $t$), $w_{fg}$ and $\sigma_{fg}^2$ represent the pixel probabilities and variance of foreground pixel class, respectively (both below threshold $t$), and $\sigma^2$ represents the within-class variance. The pixel probabilities are calculated for each pixel value in both background and foreground separated by given $t$ and are expressed as

$$\begin{aligned} w_{fg}(t) &= \sum_{i=1}^{\mathrm{T}} P(i) = \sum_{i=1}^{\mathrm{T}} \frac{n_i}{n} \\ w_{bg}(t) &= \sum_{i=t+1}^{I} P(i) = \sum_{i=t+1}^{I} \frac{n_i}{n} \end{aligned} \tag{2}$$

where $n_i$ is the number of pixels of intensity value $i$, and $n$ is the total number of pixels of the input image.

Seeded region growing technique is a region-growing segmentation method where regions are grown from a set of seed points/pixels based on similarity criterion such as similar pixel intensity. It is an iterative process that continues till all the adjacent pixels of the seed pixels are classified into respective regions.

The two-step breast tissue profile extraction is done as follows.

1) *Step 1:* The breast profile (considered as foreground) is separated from the background using threshold values obtained from Otsu's method (two classes) followed by seeded region growing with 4-connected similar intensity neighborhood pixel growth from seed pixels. The centroid pixels of the foreground and background are considered as the seed pixels.
2) *Step 2:* The breast profile obtained from step 1 has breast tissue profile and pectoral muscles. In this step,

the breast tissue profile (considered as foreground) is extracted from the pectoral muscles (considered as background) using Otsu's threshold values followed by seeded region growing with 4-connected similar intensity pixels for region growth from the seed pixels [27]. The corners pixels of the foreground and background are considered as seed pixels in this step.

The single-channel red-plane image $I_{\text{red}}$ is segmented to obtain the red-plane breast profile $I'$ which is used for further processing.

#### 3) NOISE REMOVAL FOLLOWED BY CONTRAST ENHANCEMENT

The extracted breast tissue profile is filtered using anisotropic diffusion (AD) filtering to remove unwanted noise. AD is an iterative, nonlinear partial differential equation-based technique that smoothens only on either side of the detected edge. This filtering process preserves the edges and the small objects within an image that are significant for tumor detection in a thermogram [28]. For an unfiltered red-plane breast profile $I' \in \mathbb{R}^{(P\times Q)_1}$, the AD filtering is given as

$$I'_{ss} = \text{div}\big(g(|\nabla I'|)\nabla I'\big) \tag{3}$$

where $ss$ is the scale-space parameter, $\nabla$ denotes the gradient, div(...) is the divergence operator, and $g(|\nabla I'|)$ is the edge stopping function dependent on the magnitude of the gradient. Equation (3) can be written in discrete form as

$$I_a^{'(ss+1)} = I_a^{'(ss)} + \frac{\lambda}{|\eta_a|}\sum_{b\in\eta_a} g\Big(\nabla I_{a,b}^{'(ss)}\Big)\nabla I_{a,b}^{'(ss)} \tag{4}$$

where $ss$ now denotes the number of times the filter is applied (also called as scale-space parameter as mentioned above), $I_a^{'(ss)}$ is the discrete red-plane image at the $ss$th step, and $a$ is a pixel position in a discrete, 2-D grid. The constant $\lambda$ is a scalar that determines the rate of diffusion, $\eta_a$ represents the set of adjacent pixels of $a$, and $|\eta_a|$ denotes the cardinality of the set $\eta_a$. $\nabla I_{a,b}^{'(ss)}$ represents the magnitude of the image directional gradient from pixel $a$ to $b$ at the $ss$th filtration. The directional gradient $\nabla I_{a,b}^{'(ss)}$ is approximated by $I_a^{'(ss)} - I_b^{'(ss)}$. In this work, AD filtering is implemented with eight nearest neighbor pixels (and five discrete time steps (scale-space parameter) that resulted in the final filtered red-plane image $I_f$.

This filtered red-plane breast profile $I_f \in \mathbb{R}^{(P\times Q)_1}$ is contrast-enhanced using contrast limited adaptive histogram equalization (CLAHE) [29]. It enhances the local contrast of an image making the tumor edges more prominent. CLAHE is a variant of adaptive histogram equalization that computes histograms of different sections (or regions) within an image and redistributes the intensity values within the section (or region) at a predefined clipping-limit $\beta$ [29]. In this work, the clipping limit is set to 0.01 and the clipped histograms are redistributed as a uniform distribution to produce a contrast-enhanced red-plane breast profile $I_{ce}$. This single-channel red-plane preprocessed breast thermogram $I_{ce}$ is henceforth written as $I$ in all the following sections.

**TABLE 2.** First-order statistical parameters.

| FEATURE | FORMULA |
|---|---|
| MEAN | $\mu = \frac{\sum_{i=1}^{n} x_i}{n}$ (5) where $x_i$ is the pixel intensity and $n$ is the number of pixels of $I_R$ or $I_L$ at a time. |
| VARIANCE | $\sigma^2 = \frac{\sum_{i=1}^{n}(x_i-\bar{x})^2}{n-1}$ (6) where $\sigma^2$ is the pixel variance, $x_i$ is the intensity value of each pixel, $\bar{x}$ is the mean value of all pixels and $n$ is the number of pixels of $I_R$ or $I_L$ at a time. |
| SKEWNESS | $s = \frac{\sqrt{n(n-1)}}{n-2}\frac{\frac{1}{n}\sum_{i=1}^{n}(x_i-\mu)^3}{\left(\sqrt{\frac{1}{n}\sum_{i=1}^{n}(x_i-\mu)^2}\right)^3}$ (7) where $\mu$ is the mean of all pixel intensities, $x_i$ is the intensity value of each pixel and $n$ is the number of pixels of $I_R$ or $I_L$ at a time. |
| KURTOSIS | $k = \frac{n-1}{(n-2)(n-3)}\left((n+1)\frac{\frac{1}{n}\sum_{i=1}^{n}(x_i-\mu)^4}{\left(\frac{1}{n}\sum_{i=1}^{n}(x_i-\mu)^2\right)^2} - 3(n-1)\right)+3$ (8) where $\mu$ is the mean of all pixel intensities, $x_i$ is the intensity value of each pixel and $n$ is the number of pixels of $I_R$ or $I_L$ at a time. |
| ENTROPY | $H = -\text{sum}(p.*\log_2(p))$ (9) where $p$ is the normalized histogram counts of $I_R$ or $I_L$ at a time. |

### B. FEATURE EXTRACTION FOR ASYMMETRY ANALYSIS

The temperature distribution is almost symmetrical in both breasts in a healthy individual. The angiogenesis in a budding abnormal growth alters the symmetrical temperature distribution between the breasts. These asymmetrical temperature distributions in an abnormal subject change the intensity values of each breast thereby changing the statistical and textural features of a breast thermogram.

The preprocessed red-plane breast thermogram $I \in \mathbb{R}^{(P\times Q)_1}$ is divided vertically along the center point of the thermogram into two halves (or sides) $I_{\text{side}} \in \mathbb{R}^{(P\times[Q/2])_1}$, that is, one half is left breast $I_L \in \mathbb{R}^{(P\times[Q/2])_1}$, and the other half is right breast $I_R \in \mathbb{R}^{(P\times[Q/2])_1}$, for feature extraction. In this work, statistical and textural features that highlight the asymmetry between the left and right breast are extracted.

#### 1) STATISTICAL FEATURES

The first-order statistical parameters, namely, mean, variance, skewness, kurtosis, and entropy (as described in Table 2) are calculated for each breast. These parameters serve as feature values for classification.

However, lack of spatial information makes these features fail to achieve accurate results in special cases such as the breasts of a lactating mother where asymmetry in breast temperatures is due to milk production and not due to an abnormality.

#### 2) TEXTURAL FEATURES

Textural features carry spatial information. The distinct pixel intensity patch formed by the abnormal growth has a wide variation of discrete red tone leading to a distinct texture. This texture can be ascertained by several conventional textural features such gray-level co-occurrence matrix (GLCM) and gray-level run length matrix (GLRLM) features. However, these conventional textural features are computationally expensive and they quantize the image before

calculating the features that can potentially remove relevant details for abnormality detection [30]. Nonconventional textural features such fractal texture features have shown distinct difference between a normal breast and an abnormal breast of a subject [13]. In this article, various textural features, such as FD, HE, spectral norm, and Frobenius norm for both breasts in a thermogram, are calculated individually. This work also introduces the concept of similarity of histograms between left and right breast as a textural feature for asymmetry analysis.

1) *Fractal Dimension:* FD of an image highlights self-similar patterns within an image. It provides a statistical index of complexity by comparing the changes in the pattern with that of the scale at which it is measured [31]. An abnormality in a breast changes the pattern of the thermogram as well as the FD of the image. This work calculates FD by the well-known box-counting method or reticular cell counting (RCC) method for each breast. The FD of an image is calculated as

$$\mathrm{FD} = \frac{\log(N)}{\log\left(\frac{1}{r}\right)} \tag{10}$$

where $N$ is the total number of box count each of length $L$ which is calculated using the RCC method, and $(1/r)$ is the reduction factor according to the box length.

In the RCC method [32], a red-plane one side breast thermogram of size $(P \times [Q/2])$ is reduced to various boxes of size $L \times L$ with corresponding gray levels. FD of the given thermogram is proportional to the size of the box used. The reduction factor is also dependent on the box size and is given as

$$\frac{1}{r} = \frac{P}{L}. \tag{11}$$

Each box $n \in \mathbb{R}^{L \times L \times L'}$ containing at least one gray level of the image is considered a nonempty box. The gray level of each box of size $L$ is given by

$$L' = \left\lfloor L \times \frac{G}{P} \right\rfloor \tag{12}$$

where $G$ is the total number of gray levels (or 256). Thus, the total box counts for the calculation of FD are given as

$$N = \sum_{i,j} n_r(i,j). \tag{13}$$

For an image having size $P \times (P/2)$, a box length cannot be more than the half of the image length $L \leq (P/2)$. The above procedure can be repeated using a window that moves from left to right covering the entire image [33]. The window size used in this work is 50 obtained through trial and error, for the best classification result.

2) *Hurst Exponent:* HE also known as roughness exponent represents the image pixel density fluctuations [34]. Abnormal breasts have higher image density fluctuations or surface roughness than normal breast which in turn favors asymmetry analysis. Abnormal breasts also disrupt the self-similar (or self-affine) patterns within a thermogram. For self-affine processes, HE is directly related to FD as

$$\mathrm{HE} = (n+1) - \mathrm{FD} \tag{14}$$

where FD is the fractal dimension of the one breast thermogram with $n$-dimension ($n = 2$ in our case) [35].

3) *Spectral Norm:* Norms can be used for "measuring" the similarity of two matrices and helps to quantify the differences between two matrices. The asymmetry between an abnormal and normal breast can be identified based on this norm value [36]. The norm of a matrix $A$ is analogous to vector norm and is denoted by $\|A\|_p$. A matrix norm satisfies the following conditions.

1) $\|A\|_p = 0$ if $\mathrm{A} = 0$ otherwise $\|A\| > 0$.
2) $\|kA\|_p = |k|\|A\|_p$.
3) $\|A + B\| \leq \|A\|_p + \|B\|_p$.
4) $\|AB\| \leq \|A\|_p \|B\|_p$.

In this work, the spectral or 2-norm ($p$=2) of each breast of the preprocessed breast thermogram is computed. The spectral norm of either side of breast thermogram $I_{\mathrm{side}}$ is defined as the largest singular value of $I_{\mathrm{side}}$ or the square root of the largest eigenvalue of $(I_{\mathrm{side}}^{\mathrm{T}} I_{\mathrm{side}})$, where $I_{\mathrm{side}}^{\mathrm{T}}$ denotes the transpose of $I_{\mathrm{side}}$. It can be written as

$$\|I_{\mathrm{side}}\|_2 = \left(\text{largest eigenvalue of } \left(I_{\mathrm{side}}^{\mathrm{T}} I_{\mathrm{side}}\right)\right)^{1/2}. \tag{15}$$

4) *Frobenius Norm or Hilbert–Schmidt Norm:* Frobenius norm or Hilbert–Schmidt norm can also be used to estimate the similarity between two matrices [36]. The norm values will change in case of any asymmetry between both breasts. In this work, Frobenius norm of each breast $I_{\mathrm{side}} \in \mathbb{R}^{P \times [Q/2]}$ in the preprocessed thermogram $I$ is calculated as

$$\|I_{\mathrm{side}}\|_F = \sqrt{\sum_{i=1}^{P} \sum_{j=1}^{Q/2} |x_{ij}|^2} = \sqrt{\mathrm{Tr}\left(I_{\mathrm{side}} I_{\mathrm{side}}^{\mathrm{T}}\right)} \tag{16}$$

where $x_{ij}$ is the pixel intensity of $I_{\mathrm{side}} \in \mathbb{R}^{(P \times [Q/2])_1}$, and Tr is the matrix trace of $(I_{\mathrm{side}} I_{\mathrm{side}}^{\mathrm{T}})$ which returns the sum of diagonal entries of the singular value matrix obtained from each breast thermogram $I_{\mathrm{side}}$.

5) *Histogram Similarity:* The histogram of an image is the frequency distribution of the number of pixels at different intensity levels which provides an estimate of the tonal distribution within an image. Histograms also provide the texture information within an image [37]. An abnormality in a thermogram appears as a patch of pixels with different intensity values and with a different texture. Therefore, comparing the histogram of an abnormal and a normal breast highlights the asymmetry between them thereby facilitating abnormality detection. This work introduces histogram similarity as a textural feature and measures the degree of similarity between the histogram of the left and right breast of the preprocessed breast thermogram by estimating the correlation between the

two. It is given as

$$C(H_L, H_R) = \frac{\sum_B \left(H_L(B) - \bar{H}_L\right)\left(H_R(B) - \bar{H}_R\right)}{\sqrt{\sum_B \left(H_L(B) - \bar{H}_L\right)^2 \sum_B \left(H_R(B) - \bar{H}_R\right)^2}} \tag{17}$$

where $H_L$ is the histogram of the left breast $I_L$, and $H_R$ is the histogram of the right breast $I_R$ with $B$ number of histogram bins each, $\bar{H}_L$ and $\bar{H}_R$ are the mean of histograms of left and right breast, respectively. It is given as

$$\bar{H}_k = \frac{1}{B}\sum_B H_k(B) \qquad \forall \qquad k = L, R.$$

If the value of $C(H_L, H_R)$ is almost 1 (above 0.9900), the left and right breast histograms are considered similar and both the breasts are considered symmetrical.

### C. BILATERAL RATIOS FOR ASYMMETRY ANALYSIS

The statistical and textural features extracted in the previous section differentiate an abnormal breast from a normal breast. The idea of breast abnormality detection based on asymmetry is well-known. However, this asymmetry has always been characterized by the absolute mean difference of features between the left and right breast of a grayscale thermogram. Lack of normalization is the primary disadvantage of using such difference-based asymmetry analysis [38]. This work utilizes BRs of the extracted statistical and textural features of the red-plane left and right breast thermogram for asymmetry analysis. The BR is defined as the absolute ratio of the feature value of the given breast and the feature value of the other breast. BR can be computed either as $\mathrm{BR_{LR}}$ or $\mathrm{BR_{RL}}$ and given as

$$\mathrm{BR_{LR}} = \left|\frac{\text{Feature value of left breast}}{\text{Feature value of right breast}}\right| \tag{18}$$

$$\mathrm{BR_{RL}} = \left|\frac{\text{Feature value of right breast}}{\text{Feature value of left breast}}\right| = \frac{1}{\mathrm{BR_{LR}}}. \tag{19}$$

A value of BR close to one indicates symmetry while a value of BR away from one indicates asymmetry. For each feature, if the value of either $\mathrm{BR_{LR}}$ or $\mathrm{BR_{RL}}$ is close to one, it will indicate symmetry. A subject with majority of features with symmetrical BR values is considered normal while a subject with majority of features with asymmetrical BR values is considered abnormal.

### D. CLASSIFICATION: ABNORMAL AND NORMAL

The classification algorithm used in this work is a hard voting ensemble-based classification algorithm as shown in Fig. 3. For a thermogram, the decision of classification into abnormal or normal is done by the BR ($\mathrm{BR_{LR}}$ or $\mathrm{BR_{RL}}$) of each feature individually. The decisions made by each feature individually are combined using hard voting (or majority voting) to predict the final classification. This implies that if the majority of BRs indicate asymmetry between the left and right breast, the subject is classified as abnormal while if the majority of BRs indicate symmetry between the left and right breast, the subject is classified as normal.

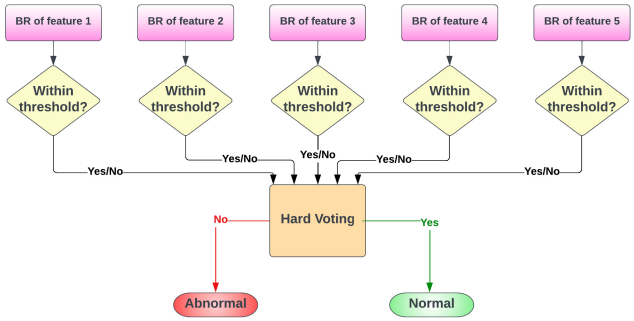


**FIGURE 3.** Hard voting ensemble-based classification algorithm.

**TABLE 3.** Details of the type and number of subjects.

| Type of subjects | Ann Arbor | DMR dataset |
|---|---|---|
| Normal non-lactating female | 3 | 26 |
| Abnormal non-lactating female | 11 | 43 |
| Normal lactating female | 1 | 0 |
| Abnormal Male | 1 | 0 |
| Total no. of subjects (85) | 16 | 69 |

In an ideal scenario, the BRs of features from symmetrical breasts of a subject should be 1. However, in real time, sweating or any other unavoidable bodily functions may cause slight elevation of temperature in certain areas of breast. This can be identified as an abnormality thereby producing high false positives. Thus, a margin of error (MOE) or threshold is introduced to bound the BR values (either $\mathrm{BR_{LR}}$ or $\mathrm{BR_{RL}}$) close to 1 for asymmetry analysis. For example, when 10% MOE is considered, BR values of all thermograms (either $\mathrm{BR_{LR}}$ or $\mathrm{BR_{RL}}$) should be less than a threshold of 1.10 to be considered symmetrical, else will be considered asymmetrical. In this work, the thresholds are varied from 1 to 1.15 (0% MOE to 15% MOE) and classification accuracy is calculated at each threshold value. An optimum threshold (or MOE) is obtained when the classification accuracy is maximum. A detailed analysis of the effect of threshold variation on classification accuracy is shown in Section III.

## III. EXPERIMENTATION

### A. DATASET USED

A total of 85 breast thermograms taken from Ann Arbor thermography [39] and DMR, Visual Lab [40] has been used for experimentation in this work. These thermograms are standardized front view thermal images (containing both breasts) of size 640 × 480 pixels. Diagnosis is available in all cases. The dataset-wise and subject-wise details of the 85 thermograms used are given in Table 3.

The DMR database was recorded with a FLIR SC-620 thermal camera that has a sensitivity of less than 0.04 °C and range of capture of –40 °C to 500 °C, however, the details of the infrared camera used in Ann Arbor thermography

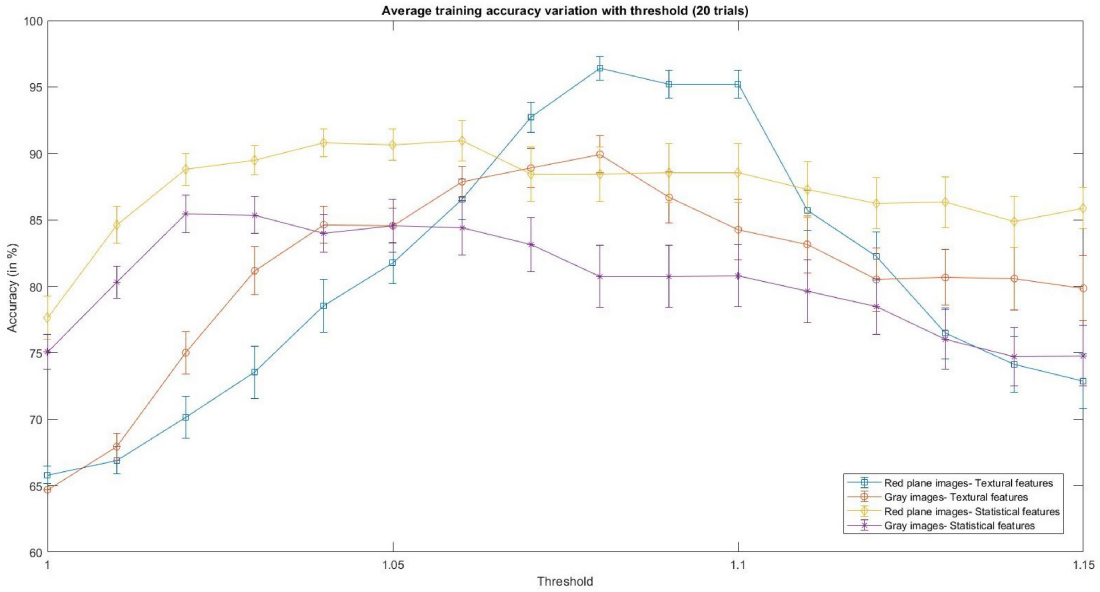


**FIGURE 4.** Average training accuracy variation with threshold over 20 trials.

are not available. Both the databases were collected following the preexamination preparation protocols outlined by AAT [24].

### B. RESULTS

Repeated hold-out cross-validation technique is used to test the performance of the proposed methodology. In this cross-validation technique, an 80%–20% random split of the dataset into training and testing is done and the split is repeated for several trials. To provide an exhaustive analysis of the proposed methodology, classification performance using statistical and textural features is evaluated. A comparison of grayscale images and red-plane images has also been done to highlight the superiority of using red-plane for abnormality detection. All experiments were performed on MATLAB 2021b.

#### 1) THRESHOLD VARIATION

The training dataset is used to estimate optimum threshold value. The threshold is varied from 1 to 1.15 and at each threshold value, training accuracy is calculated. The threshold value at which the training accuracy is maximum is considered as optimum threshold. This optimum threshold is used to test the performance of the proposed methodology on the testing dataset. The dataset random split is repeated and the performance of the proposed methodology is evaluated over 20 trials. The performance metrics, namely, accuracy, sensitivity, specificity, and F1-score, is obtained at each threshold value. Fig. 4 shows the average training accuracy with standard deviation of the proposed methodology at each threshold value over 20 trials using red-plane and grayscale images with statistical and textural features. Similarly, Figs. 5–7 show average training sensitivity, average training specificity, and average training F1-score, respectively.

It is observed in Fig. 4 that, for all cases, the average training accuracy increases with increase in threshold values and reaches a maximum at optimum threshold. Further increment of threshold value decreases the average training accuracy. The optimum threshold value obtained at each trial is used to evaluate the performance of the proposed methodology with the testing dataset. Fig. 5 shows that the average training sensitivity increases with the increase in threshold values and then saturates after a particular threshold value while Fig. 6 depicts the decrease of average training specificity with the threshold values. The threshold variation from 1 to 1.15 helps to achieve a balance between sensitivity and specificity. Average training F1-score as seen in Fig. 7 has a similar trend as that of average training accuracy. From the above figures, it is seen that the red-plane thermograms with textural features have the best training performance metrics.

#### 2) PERFORMANCE METRICS

The optimum threshold obtained in each trial with training data is used to test the performance of the proposed methodology with the testing dataset. Table 4 shows the average performance metrics of the proposed methodology with standard deviation for abnormality detection over 20 trials.

It is observed that red-plane images with textural features have the highest accuracy, sensitivity, specificity, and F1-score with least standard deviation. Grayscale images with textural features perform slightly better than red-plane images with statistical features but with a larger standard deviation. It can be observed that the red-plane images have significantly higher average performance metrics with lower standard deviation when

**TABLE 4.** Performance metrics of abnormality detection using statistical and textural features on testing data at optimum thresholds.

| Features → | Statistical | | Textural | |
|---|---|---|---|---|
| Metrics ↓ | Gray images | Red-plane images | Gray images | Red-plane images |
| Accuracy (in %) | 85.59 ± 7.01 | 89.41 ± 5.60 | 91.47 ± 5.87 | 96.08 ± 3.87 |
| Sensitivity (in %) | 87.01 ± 5.54 | 90.48 ± 4.43 | 94.74 ± 5.21 | 100 ± 0 |
| Specificity (in %) | 86.77 ± 15.64 | 89.95 ± 11.12 | 88.26 ± 12.21 | 93.57 ± 7.29 |
| F1-score (in %) | 89.00 ± 5.87 | 92.00 ± 5.18 | 93.20 ± 4.90 | 96.62 ± 3.23 |

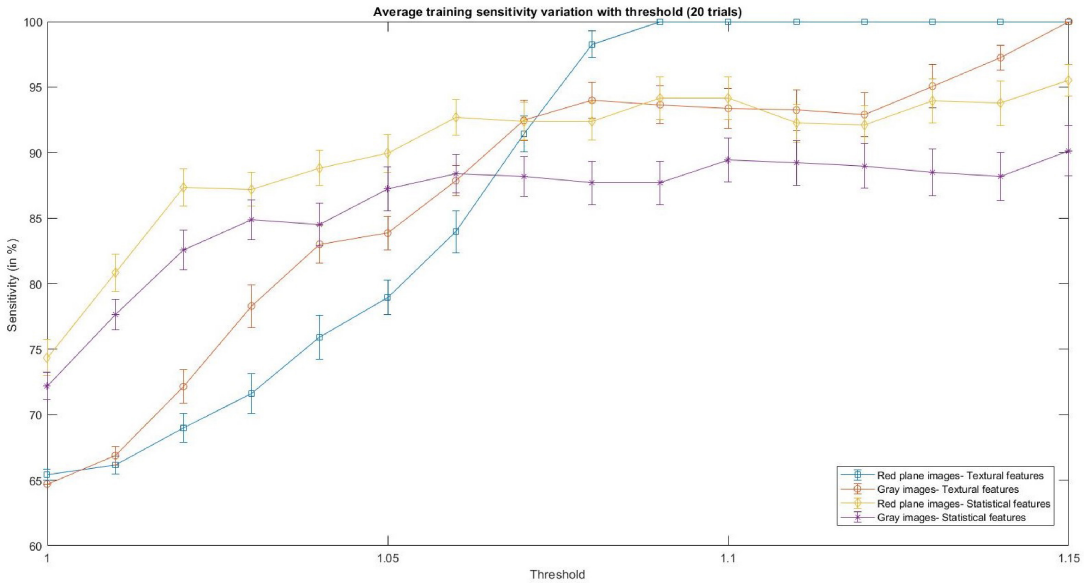


**FIGURE 5.** Average training sensitivity variation with threshold over 20 trials.

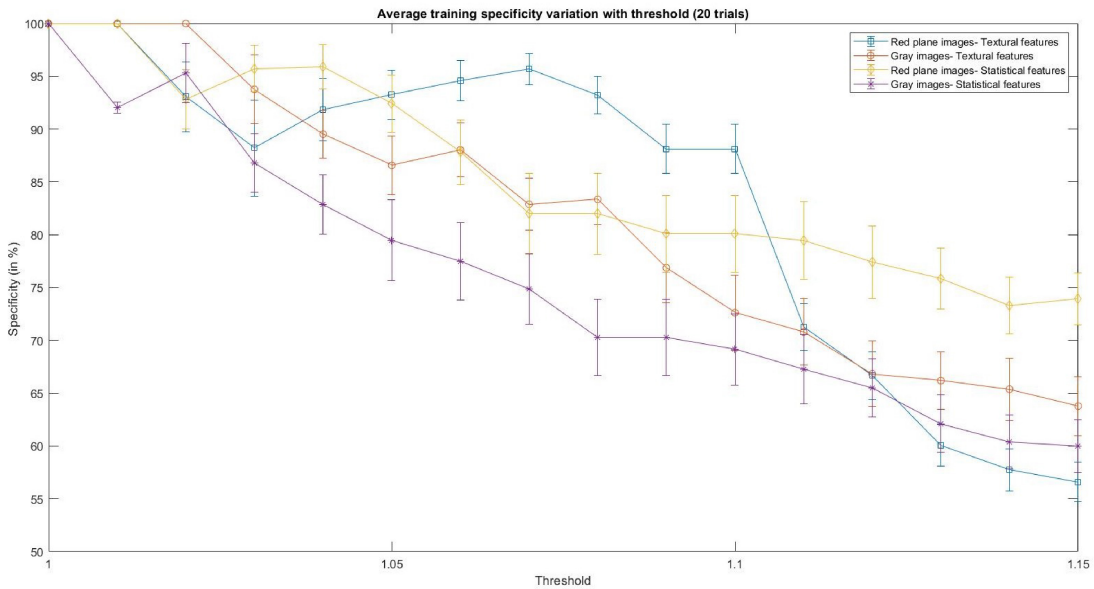


**FIGURE 6.** Average training specificity variation with threshold over 20 trials.

compared to grayscale images. Textural features improve the classification performance significantly when compared to statistical features irrespective of grayscale or red-plane breast thermograms. The proposed methodology achieved the best average performance in terms of accuracy, sensitivity, specificity, F1-score, and the lowest standard

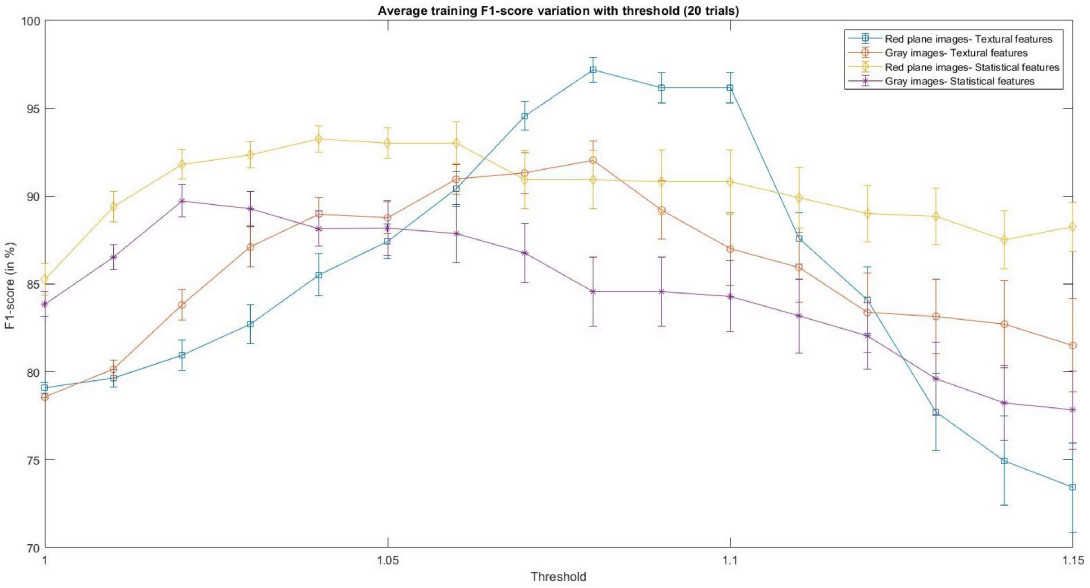


**FIGURE 7.** Average training F1-score variation with threshold over 20 trials.

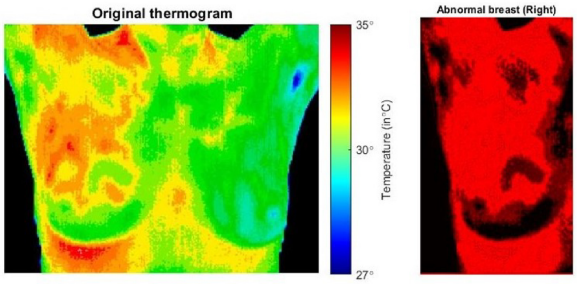


**FIGURE 8.** Identification of right abnormal breast.

deviation with proposed textural features for red-plane breast thermograms.

## IV. IDENTIFICATION OF THE ABNORMAL BREAST OF ABNORMAL SUBJECT

In this work, a novel singular value-based method is introduced to identify the abnormal breast of the detected abnormal subject. SVD of the left and right breast of the abnormal subject is performed. SVD is a form of factorization such that

$$I_{\text{side}} = U_{\text{side}} \Sigma_{\text{side}} V_{\text{side}}^{\text{T}} \tag{20}$$

where $U_{\text{side}}$ and $V_{\text{side}}$ are orthonormal matrices, and $\Sigma_{\text{side}}$ is a diagonal matrix. The real, non-negative diagonal entries of $\Sigma$ are square roots of the eigenvalues of $I_{\text{side}}^{\text{T}} I_{\text{side}}$ and are called singular values. The singular values $\sigma_i$ are usually sorted in decreasing order so that $\Sigma = \text{diag}(\sigma_1, \sigma_2, \ldots, \sigma_{[Q/2]})$ with $\sigma_1 \geq \sigma_2 \geq \cdots \geq \sigma_{[Q/2]} \geq 0$. $I_{\text{side}}$ is said to have a rank $r_{\text{side}}$ if the SVD of $I_{\text{side}}$ has $r$ number of nonzero components. The large singular values contain more image information as compared to small (near 0) singular values. An image with no edges has less information or a smaller number of large singular values whereas an image with edges or sudden changes in pixel intensities has more information or greater number of large singular values [41]. The decay of singular values in an image with edges is slower as compared to the decay of singular values in an image with no edges. Thus, a breast with abnormality (tumor edges present) will have a slower decay of singular values as compared to a breast without abnormality. In this work, this idea for abnormal breast identification of an abnormal subject is exploited. After the proposed methodology detects an abnormal subject, SVD is done for both the breasts. The decay $D$ is estimated by calculating the difference of the first and second singular values normalized by the first singular value for each breast

$$D = \frac{\sigma_1 - \sigma_2}{\sigma_1}. \tag{21}$$

The breast with the lower decay value $D$ is classified as the abnormal breast.

**if** $D$ of left breast $<$ $D$ of right breast **then**
  Abnormal breast: Left
**else if** $D$ of right breast $<$ $D$ of left breast **then**
  Abnormal breast: Right
**end if**

For the thermogram of the subject along with their detected right abnormal breast based on the proposed methodology shown in Fig. 8, the first two singular values and the decay of the values $D$ of each breast, are presented in Table 5. The $D$ of the right abnormal breast is lower than that of the left normal breast. Similarly, the thermogram of another subject with their detected left abnormal breast based on the proposed methodology is shown in Fig. 9 and its corresponding first two singular values and the decay of the value is shown in Table 6. The $D$ value of the

**TABLE 5.** SVD values for a subject with right abnormal breast in Fig. 8.

| Red-plane Image | $\sigma_1$ | $\sigma_2$ | $D$ |
|---|---|---|---|
| **Left Breast** | 209.7732 | 38.9855 | 0.8142 |
| **Right Breast** | 110.2271 | 47.9264 | 0.5652 |

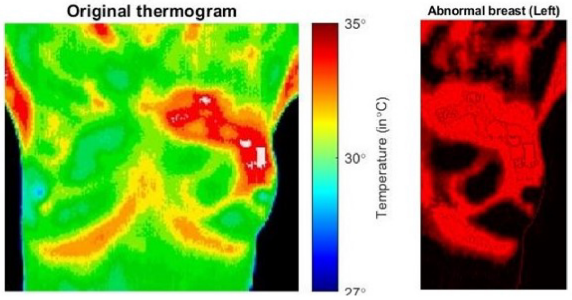


**FIGURE 9.** Identification of left abnormal breast.

**TABLE 6.** SVD values for a subject with left abnormal breast in Fig. 9.

| Red-plane Image | $\sigma_1$ | $\sigma_2$ | $D$ |
|---|---|---|---|
| **Left Breast** | 93.0563 | 40.3399 | 0.5665 |
| **Right Breast** | 125.2968 | 41.4004 | 0.6696 |

left abnormal breast is lower than that of the right normal breast.

However, these figures only show preliminary results for abnormal breast identification because of the lack of ground truth for identification of abnormal breast in the DMR dataset. The observations are validated based on the ground truth available for the Ann Arbor thermography dataset. The observations were validated on all the 16 subjects available in the Ann Arbor thermography dataset, reaching an accuracy of 98%.

## V. COMPARISON WITH RECENT STATE-OF-THE-ART

Out of all the state-of-the-art works shown in Table 1, [15] achieves the highest accuracy of breast abnormality detection of 95%. In this work, an extensive comparison with [15], the best performing state-of-the-art is presented.

In [15], a novel asymmetry-based methodology using segmented region of interest (ROI) to identify subjects with abnormal breasts is proposed. In this state-of-the-art, the breasts were extracted together using vertical and horizontal projections. (Readers are directed to [15] for more details.) Following this, the extracted breasts were segmented using a bifurcation point between the breasts obtained by interpolating and fitting infra-mammary curves (or Catenary curves) on both breasts. The obtained bifurcation point was used as the point of division of the left and right breast for asymmetry analysis. After bifurcation, the so-obtained breasts were considered as ROI. The absolute difference of statistical parameters of the extracted ROI, such as mean, variance, skewness, kurtosis, and entropy, were used as features. An SVM classifier was used for the classification of normal and abnormal breasts.

In order to evaluate the state-of-the-art, the same dataset used in this article was considered. An 80%–20% split of the data was done to form the training and the testing sets. Five different trials were conducted by doing random 80%–20% splits of the data to form five different training and testing sets. The following experiments were performed to extensively compare with [15].

1) *Model-1:* Reimplementation of the algorithm in [15] with the dataset used in this work.
2) *Model-2:* Breast segmentation using the curve segmentation technique in [15] followed by the proposed methodology of this article.
3) *Model-3:* Breast segmentation given in Section II-A2 with the classification algorithm using an absolute difference of features as proposed in [15].

An advantage of the proposed work is the utilization of global features as compared to the majority of work in [7], [11], and [15], that uses local features from the ROI for classification. The estimation of correct ROI for feature extraction is extremely controversial without appropriate ground truths. It can be speculated that using bifurcation points for the division of the left and right breast may be advantageous, however, the comparison results (Model-2 and Model-3) suggest that such calculations unnecessarily augment the complexity of the methodology. The computational complexity of the proposed classification algorithm is $O(1)$ while the computational complexity of the state-of-the-art SVM classifier is $O(n^2)$ (where $n$ is the number of training samples). The following observations can be made from the detailed comparison shown in Table 7.

1) The performance of the algorithm in [15] when reimplemented is found significantly inferior to the performance of the proposed methodology in this work.
2) The performance of the ML model [with a computational complexity of $O(n^2)$] in [15] is similar to the performance of the proposed non-machine learning threshold-based methodology [with a computational complexity of $O(1)$] using the statistical features of gray images. This indicates that the proposed non-ML methodology which has significantly less computational complexity can perform at par with the state-of-the-art ML technique.
3) The performance of the proposed methodology with the curve segmentation technique used in [15] (Model-2) is found slightly inferior to the performance of the proposed methodology without curve segmentation. This may be due to the presence of unique subjects in the dataset used such as a subject with mastectomy done or a male subject for which the catenary curves fail to segment breasts (due to the absence of curvature).

**TABLE 7.** Comparison of performance with [15] (all metrics in %).

| Features → | Statistical | | Textural | |
|---|---|---|---|---|
| **Models ↓** | **Gray images** | **Red-plane images** | **Gray images** | **Red-plane images** |
| **Model-1** | Accuracy= 84.70 ± 5.26<br>Sensitivity= 84.62 ± 5.31<br>Specificity= 76.67 ± 11.13<br>F1-score= 84.62 ± 5.31 | Not applicable | Not applicable | Not applicable |
| **Model-2** | Accuracy= 84.71 ± 6.89<br>Sensitivity= 89.4 ± 6.66<br>Specificity= 78.33 ± 12.94<br>F1-score= 88.04 ± 5.07 | Accuracy= 88.75 ± 7.18<br>Sensitivity= 88.02 ± 6.01<br>Specificity= 90.33 ± 10.91<br>F1-score= 91.60 ± 6.37 | Accuracy= 87.50 ± 5.69<br>Sensitivity= 86.47 ± 5.53<br>Specificity= 90.00 ± 9.36<br>F1-score= 91.80 ± 7.44 | Accuracy= 89.75 ± 5.80<br>Sensitivity= 94.55 ± 4.98<br>Specificity= 90.00 ± 8.94<br>F1-score= 91.39 ± 5.62 |
| **Model-3** | Accuracy= 78.75 ± 5.59<br>Sensitivity= 77.36 ± 5.66<br>Specificity= 90.33 ± 14.91<br>F1-score= 86.45 ± 6.39 | Accuracy= 83.75 ± 6.48<br>Sensitivity= 82.18 ± 6.52<br>Specificity= 90.02 ± 13.58<br>F1-score= 89.40 ± 5.91 | Accuracy= 86.25 ± 6.15<br>Sensitivity= 85.05 ± 7.81<br>Specificity= 90.00 ± 11.18<br>F1-score= 90.92 ± 5.38 | Accuracy= 87.50 ± 5.84<br>Sensitivity= 89.67 ± 6.91<br>Specificity= 89.33 ± 10.27<br>F1-score= 91.06 ± 4.69 |

4) The performance of the proposed methodology with the absolute difference of the statistical and textural features (Model-3) is significantly inferior to the performance of the proposed methodology with the BRs of the features. This confirms the superiority of BRs of the features over the absolute difference of the ratios for classification purposes.

From the above observations, it can be concluded that the proposed methodology in this work outperforms the state-of-the-art in terms of performance with less computational complexity. It can be applied in data-limited and resource-limited real-life scenarios.

## VI. CONCLUSION

This pilot study proposes a novel, computationally inexpensive, threshold-based non-learning methodology using red-plane asymmetry analysis of breast thermograms for breast abnormality detection. The BRs of several known textural features, such as FD, HE, spectral and Frobenius norm along with a novel histogram similarity-based textural feature, have been proposed for asymmetry analysis of breast thermograms. An extensive comparative analysis between the textural features and statistical features of red-plane and grayscale thermograms has been presented. Textural features of the red-plane of RGB breast thermogram have been used for abnormality detection and are shown to be better than statistical features. Abnormality detection results obtained using red-plane thermograms was considerably higher than those obtained using grayscale thermograms. An exhaustive comparison with the current state-of-the-art has also been provided to show the superiority of the proposed methodology. The proposed methodology was evaluated on two publicly available datasets, namely, DMR dataset and Ann Arbor thermography dataset and it outperformed the current state-of-the-art, achieving an accuracy of 96.08%, sensitivity of 100%, specificity of 93.57%, and F1-score of 96.62%. A novel SVD-based technique to detect the abnormal breast of an abnormal subject has also been proposed. This technique has been validated on limited dataset with available ground truth achieving an accuracy of 98%. Further validation with more datasets with adequate ground truths will be investigated as part of future work. Modifications of the proposed methodology for SBBC identification along with a detailed noise analysis, different color domain analysis, fuzzy-rule-based threshold selection, and feature importance, will be conducted as future work along with the order of importance of the features.

## REFERENCES

[1] "Breast cancer facts and statistics." Breastcancer.org. Accessed: Oct. 10, 2022. [Online]. Available: https://www.breastcancer.org/facts-statistics

[2] "Breast cancer." who.int. Accessed: Oct. 10, 2022. [Online]. Available: https://www.who.int/news-room/fact-sheets/detail/breast-cancer

[3] "Early detection." nationalbreastcancer.org. Accessed: Oct. 10, 2022. [Online]. Available: https://www.nationalbreastcancer.org/early-detection-of-breast-cancer

[4] R. Lugano, M. Ramachandran, and A. Dimberg, "Tumor angiogenesis: Causes, consequences, challenges and opportunities," *Cellular Mol. Life Sci.*, vol. 77, no. 9, pp. 1745–1770, 2020.

[5] A. A. Khan and A. S. Arora, "Thermography as an economical alternative modality to mammography for early detection of breast cancer," *J. Healthcare Eng.*, vol. 2021, pp. 1–8, Jul. 2021.

[6] S. H. Heywang-Kobrunner, A. Hacker, and S. Sedlacek, "Advantages and disadvantages of mammography screening," *Breast Care*, vol. 6, no. 3, pp. 199–207, 2011.

[7] S. V. Francis, M. Sasikala, and S. Saranya, "Detection of breast abnormality from thermograms using curvelet transform based feature extraction," *J. Med. Syst.*, vol. 38, no. 4, p. 23, 2014.

[8] S. V. Francis, M. Sasikala, G. B. Bharathi, and S. D. Jaipurkar, "Breast cancer detection in rotational thermography images using texture features," *Infrared Phys. Technol.*, vol. 67, pp. 490–496, Nov. 2014.

[9] B. Krawczyk, G. Schaefer, and M. Woźniak, "A hybrid cost-sensitive ensemble for imbalanced breast thermogram classification," *Artif. Intell. Med.*, vol. 65, no. 3, pp. 219–227, 2015.

[10] T. Gaber et al., "Thermogram breast cancer prediction approach based on neutrosophic sets and fuzzy c-means algorithm," in *Proc. Int. Conf. IEEE Eng. Med. Biol. Soc.*, 2015, pp. 4254–4257.

[11] D. Sathish, S. Kamath, K. Prasad, R. Kadavigere, and R. J. Martis, "Asymmetry analysis of breast thermograms using automated segmentation and texture features," *Signal, Image Video Process.*, vol. 11, no. 4, pp. 745–752, 2017.

[12] R. Rastghalam and H. Pourghassem, "Breast cancer detection using MRF-based probable texture feature and decision-level fusion-based classification using HMM on thermography images," *Pattern Recognit.*, vol. 51, pp. 176–186, Mar. 2016.
[13] S. Pramanik, D. Bhattacharjee, and M. Nasipuri, "Texture analysis of breast thermogram for differentiation of malignant and benign breast," in *Proc. Int. Conf. Adv. Comput., Commun. Inform.*, 2016, pp. 8–14.
[14] J. S. Jeyanathan, A. Shenbagavalli, B. Venkatraman, and M. Menaka, "Analysis of breast thermograms in lateral views using texture features," in *Proc. IEEE Region 10 Conf.*, 2018, pp. 2017–2022.
[15] R. R. Devi and G. S. Anandhamala, "Analysis of breast thermograms using asymmetry in infra-mammary curves," *J. Med. Syst.*, vol. 43, no. 6, p. 146, 2019.
[16] S. Pramanik, D. Bhattacharjee, M. Nasipuri, and O. Krejcar, "LINPE-BL: A local descriptor and broad learning for identification of abnormal breast thermograms," *IEEE Trans. Med. Imag.*, vol. 40, no. 12, pp. 3919–3931, Dec. 2021.
[17] M. Mejdahl et al., "Breast cancer mortality in synchronous bilateral breast cancer patients," *Brit. J. Cancer*, vol. 120, pp. 761–767, Feb. 2019.
[18] H. Zerouaoui and A. Idri, "Reviewing machine learning and image processing based decision-making systems for breast cancer imaging," *J. Med. Syst.*, vol. 45, no. 1, p. 8, 2021.
[19] M. A. S. A. Husaini, M. H. Habaebi, S. A. Hameed, M. R. Islam, and T. S. Gunawan, "A systematic review of breast cancer detection using thermography and neural networks," *IEEE Access*, vol. 8, pp. 208922–208937, 2020.
[20] U. R. Gogoi, M. K. Bhowmik, A. K. Ghosh, D. Bhattacharjee, and G. Majumdar, "Discriminative feature selection for breast abnormality detection and accurate classification of thermograms," in *Proc. Int. Conf. Innov. Electron., Signal Process. Commun.*, 2017, pp. 39–44.
[21] A. Hakim and R. N. Awale, "Identification of breast abnormality from thermograms based on fractal geometry features," in *Proc. IoT Smart Syst.*, 2022, pp. 393–401.
[22] "Picking a thermal color palette." flir.ca. Accessed: Nov. 10, 2022. [Online]. Available: https://www.flir.ca/discover/industrial/picking-a-thermal-color-palette/
[23] A. Dey and S. Rajan, "Red-plane asymmetry analysis of breast thermograms for cancer detection," in *Proc. IEEE Int. Symp. Med. Meas. Appl.*, 2022, pp. 1–6, doi: 10.1109/MeMeA54994.2022.9856520.
[24] "Guidelines: Breast thermography." aathermology.org. Accessed: Nov. 10, 2022. [Online]. Available: https://aathermology.org/organization-2/guidelines/
[25] A. Makandar and B. Halalli, "Pre-processing of mammography image for early detection of breast cancer," *Int. J. Comput. Appl.*, vol. 144, no. 3, pp. 11–15, 2016.
[26] N. Otsu, "A threshold selection method from gray level histograms," *IEEE Trans. Syst., Man, Cybern.*, vol. 9, pp. 62–66, Jan. 1979.
[27] P. K. Jain and S. Susan, "An adaptive single seed based region growing algorithm for color image segmentation," in *Proc. Annu. IEEE India Conf.*, 2013, pp. 1–6.
[28] P. Perona and J. Malik, "Scale-space and edge detection using anisotropic diffusion," *IEEE Trans. Pattern Anal. Mach. Intell.*, vol. 12, pp. 629–639, Jul. 1990.
[29] S. M. Pizer et al., "Adaptive histogram equalization and its variations," *Comput. Vis., Graph., Image Process.*, vol. 39, no. 3, pp. 355–368, 1987.
[30] D. A. Clausi and M. E. Jernigan, "A fast method to determine co-occurrence texture features," *IEEE Trans. Geosci. Remote Sens.*, vol. 36, no. 1, pp. 298–300, Jan. 1998.
[31] A. Ranganath, M. R. Senapati, and P. K. Sahu, "Estimating the fractal dimension of images using pixel range calculation technique," *Vis. Comput.*, vol. 37, pp. 635–650, Mar. 2021.
[32] A. K. Bisoi and J. Mishra, "On calculation of fractal dimension of images," *Pattern Recognit. Lett.*, vol. 22, no. 6, pp. 631–637, 2001.
[33] C. Shi, G. Ji, and Y. Wang, "Study of texture images classification method based on fractal dimension calculation," in *Proc. Int. Joint Conf. Artif. Intell.*, 2009, pp. 488–491.
[34] M. Dlask and J. Kukal, "Hurst exponent estimation of fractional surfaces for mammogram images analysis," *Physica A, Stat. Mechan. Appl.*, vol. 585, Jan. 2022, Art. no. 126424.
[35] B. Abay, "Exploration of the relationship between the fractal dimension of microcalcification clusters and the hurst exponent of background tissue disruption in mammograms," Ph.D. dissertation, Dept. Comput. Sci., Harvard Univ., Cambridge, MA, USA, 2010.
[36] J. M. Blackledget, "Chapter 8—Vector and matrix norms," in *Digital Signal Processing*, (Woodhead Publishing Series in Electronic and Optical Materials), 2nd ed. Sawston, U.K.: Woodhead Publ., 2006, pp. 208–236. [Online]. Available: https://www.sciencedirect.com/science/article/pii/B9781904275268500099
[37] K. K. Agwu and C. C. Ohagwu, "Histogram-based texture characterization and classification of brain tissues in non-contrast CT images of stroke patients," in *Pattern Recognition*. Rijeka, Croatia: IntechOpen, 2016, ch. 5. [Online]. Available: https://doi.org/10.5772/65349
[38] U. R. Gogoi, G. Majumdar, M. K. Bhowmik, and A. K. Ghosh, "Evaluating the efficiency of infrared breast thermography for early breast cancer risk prediction in asymptomatic population," *Infrared Phys. Technol.*, vol. 99, pp. 201–211, Jun. 2019.
[39] "Breast screening." aathermography.com. Accessed: Oct. 10, 2022. [Online]. Available: http://aathermography.com/breast/breasthtml/breasthtml.html
[40] L. F. Silva et al., "A new database for breast research with infrared image," *J. Med. Imag. Health Inform.*, vol. 4, no. 1, pp. 92–100, 2014.
[41] G. Strang, "Chapter 7—The singular value decomposition (SVD)," in *Introduction to Linear Algebra*, 5th ed. Wellesley, MA, USA: Wellesley-Cambridge Press, 2016, pp. 364–392. [Online]. Available: https://math.mit.edu/∼gs/linearalgebra/

**ANKITA DEY** (Graduate Student Member, IEEE) received the B.Tech. degree in electronics and communication engineering from the Maulana Abul Kalam Azad University of Technology, Kolkata, India, in 2018, and the M.Tech. degree in biomedical engineering from the Indian Institute of Technology Ropar, Rupnagar, India, in 2020. She is currently pursuing the Ph.D. degree in electrical and computer engineering with Carleton University, Ottawa, ON, Canada.

Her research interests include biomedical signal processing, biomedical image processing, machine learning for signal analysis, compressive sensing, and nondestructive evaluation.

**EBRAHIM ALI** (Graduate Student Member, IEEE) received the B.Sc. and M.Sc. degrees in biomedical engineering from Cairo University, Cairo, Egypt, in 2013 and 2017, respectively. He is currently pursuing the Ph.D. degree in electrical and computer engineering with the Department of Systems and Computer Engineering, Carleton University, Ottawa, ON, Canada.

His main research interests include deep learning, machine learning, biomedical signal and image analysis, and computer vision.

Mr. Ali is a member of IEEE Young Professionals, IEEE Signal Processing, Instrumentation and Measurement, and Engineering in Medicine and Biology Societies.

**SREERAMAN RAJAN** (Senior Member, IEEE) received the B.E. degree in electronics and communications from Bharathiyar University, Coimbatore, India, in 1987, the M.Sc. degree in electrical engineering from Tulane University, New Orleans, LA, USA, in 1992, and the Ph.D. degree in electrical engineering from the University of New Brunswick, Fredericton, NB, Canada, in 2004.

From 1986 to 1990, he was a Scientific Officer with the Reactor Control Division, Bhabha Atomic Research Center (BARC), Mumbai, India, after undergoing an intense training in nuclear science and engineering from its training school. At BARC, he developed systems for control, safety, and regulation of nuclear research and power reactors. From 1997 to 1998, he carried out research under a grant from Siemens Corporate Research, Princeton, NJ, USA. From 1999 to 2000, he was with JDS Uniphase, Ottawa, ON, Canada, where he worked on optical components and the development of signal processing algorithms for advanced fiber-optic modules. From 2000 to 2003, he was with Ceyba Corporation, Ottawa, where he developed channel monitoring, dynamic equalization, and optical power control solutions for advanced ultralong haul and long-haul fiber-optic communication systems. In 2004, he was with Biopeak Corporation, Ottawa, where he developed signal processing algorithms for noninvasive medical devices. From December 2004 to June 2015, he was a Defense Scientist with the Defence Research and Development Canada, Ottawa. He joined the Department of Systems and Computer Engineering, Carleton University, Ottawa, as a Tier 2 Canada Research Chair (Advanced Sensors Systems and Signal Processing) in July 2015, where he is currently a Full Professor. He was the Director of the Ottawa-Carleton Institute for Biomedical Engineering (OCIBME), Carleton University from 2020 to 2022. He was an Adjunct Professor with the School of Electrical Engineering and Computer Science, University of Ottawa, Ottawa, from July 2010 to June 2018, and has been an Adjunct Professor with the Department of Electrical and Computer Engineering, Royal Military College, Kingston, ON, Canada, since July 2015. He is the holder of two patents and two disclosures of invention. He is an author of more than 200 journal articles and conference papers. His research interests include signal and image processing, biomedical signal processing, pattern classification, and applied machine learning.

Prof. Rajan was awarded the IEEE MGA Achievement Award in 2012 and recognized for his IEEE contributions with Queen Elizabeth II Diamond Jubilee Medal in 2012. IEEE Canada recognized his outstanding service through 2016 W.S. Read Outstanding Service Award. He has been involved in organizing several successful IEEE conferences and has been a reviewer for several IEEE journals and conferences. He is currently the Chair of the IEEE Ottawa EMBS and AESS Chapters. He has been the North America Regional Director for IEEE Consumer Technology Society since 2021 and is the Member-at-Large in its Board of Governors. He has served IEEE Canada as its Board Member from 2010 to 2018.